BUTTERWORTH HEINEMANN

Polymer Vol. 36 No. 7, pp. 1383–1392, 1995

0032-3861/95/$10.00 + 0.00

Tensile, stress relaxation and dynamic mechanical behaviour of polyethylene crystallized from highly deformed melts

Yu. M. Boiko
Physico-Mechanical Laboratory, Plastpolymer Okhta Research and Production Association, Polustovsky Prospekt 32, 195108 St Petersburg, Russia

Witold Brostow* and Anatoly Ya. Goldman
Center for Materials Characterization and Department of Physics, University of North Texas, Denton, TX 76203-5308, USA

and A. C. Ramamurthy
Automotive Components Group, Ford Motor Co., 24300 Glendale Avenue, Detroit, MI 48239, USA
(Received 8 July 1994; revised 26 August 1994)

High-density polyethylene (HDPT) specimens were obtained by standard extrusion and also by a procedure of solidification from a highly deformed melt (Sodem) in wide ranges of temperature T, time t, and draw ratio λ from 1.0 to 12.2. Tensile tests were conducted isothermally between 20 and 120°C and stress relaxation at constant tensile strain studied as a function of time also isothermally at several temperatures in the range from −50 to +100°C. Dynamic mechanical testing was similarly conducted in the range from −150 to +120°C. The time–temperature equivalence principle, an equation for the temperature shift factor a_T as a function of the reduced volume $\tilde{v}$ and the Hartmann equation of state were applied to the properties so established, including the stress relaxation and the mechanical loss tangent. The earlier shift factor equation has been generalized so that it now includes the draw ratio in two ways: $\ln a_T = 1/[a + c\lambda] + B/[\tilde{v} - 1]$; a, c and the Doolittle constant B are characteristic for a given material but independent of the degree of orientation and of temperature. The reduced volume $\tilde{v}$ depends on temperature T via equation (7) and on λ via equation (8). Drawing causes a decrease in the number of available chain conformations, which is reflected in the first term; it also changes intersegmental interactions, as reflected in the second term through equation (8). The Sodem procedure improves mechanical properties of HDPE. Specimens with the highest draw ratio $\lambda = 12.2$ exhibit the highest elastic modulus and the highest tensile strength as well as high relaxation rates during long-term testing.

INTRODUCTION

There are at least three approaches in the quest for polymeric materials with improved properties. The first is synthesis, the second is blending and manipulation of properties of *existing* polymers by variations of molecular masses and details of molecular structures (such as branching), and the third is by designing new processing regimes. The last approach – exemplified by dealing with a material such as polyethylene (PE) on which so much work has been done already – might well be the most challenging.

Taking the third approach is well justified by both fundamental and practical considerations. Property improvement cannot be achieved here without advancing our understanding of structure, interactions and property relationships. At the same time, when properties of massively produced engineering polymers (EPs) are improved, the range of applications of thermoplastics increases, possibly in a dramatic way, without major changes in manufacturing processes. This is important for several branches of industry, including the automobile industry which is in the process of gradually replacing metal parts and components by those made from EPs.

The present work is concerned with PE, the most ubiquitous of EPs. We have already dealt with rapid crack propagation (RCP)[1] and slow crack propagation (SCP)[2] in PE, two vastly different phenomena. Important work on improving properties of PE is related to the elucidation of the structure of the crystal–amorphous phase boundary and the role of tie molecules[3–7]. As noted by Lustiger and Ishikawa[6], tie molecules constitute a 'glue' that holds the crystalline regions together. The approach taken in this work is different, and appears complementary to that just described: we deform the material to increase the orientation. Our results in

* To whom correspondence should be addressed

enhancing the mechanical properties of polymer liquid crystals (PLCs) by increasing the orientation[8] have encouraged us to attempt something similar for polyethylene. Of course, orientation of EPs is hardly a new concept[9]. There exist various solid-state procedures such as hydrostatic extrusion[10], drawing through a conical die[11], cold rolling and drawing[12] or multistage zone drawing[13]. There exists a well known method developed by Mead *et al.*[14] of creation of stretched structures of a solid under combined effects of pressure and shear in an Instron-type capillary rheometer. We have decided to concentrate on the molten state, where states of higher deformation than in the solid should be accessible. Moreover, a single-stage drawing operation would involve only relatively simple equipment and could be implemented on a large scale.

To assure reliable prediction of long-term behaviour from short-term tests, we apply the time–temperature correspondence principle[15–18]. More specifically, we apply an $a_T[v^f(T)]$ equation relating the temperature shift factor a_T to the temperature T via free volume v^f (refs 19, 20). We also use the Hartmann equation of state, known to be applicable to a large range of materials including polymer solids and liquids[21–23]; see also refs 24 and 25.

EXPERIMENTAL

Material and deformation procedures

We have used high-density PE (HDPE) made by PORPA (Plastpolymer Okhta Research and Production Association) with a density of $0.952\,g\,cm^{-3}$ determined by flotational Archimedes principle titration. The melt flow index (MFI) is 0.5 g/10 min at 190°C. The weight-average molecular mass (M_w) determined by gel-permeation chromatography (g.p.c.) with a Waters GPC-200 apparatus was 1.75×10^5, the number-average molecular mass (M_n) obtained by the same procedure was 1.60×10^4. The specific heat capacity at 25°C determined by differential scanning calorimetry (d.s.c.) with a Perkin–Elmer DSC-7 apparatus was $170\,J\,g^{-1}\,K^{-1}$. The material was extruded through a laboratory extruder.

In addition to specimens obtained by standard extrusion, we have also applied a procedure of solidification from a highly deformed melt, which will be referred to as Sodem. The deformation is applied to molten material but at a temperature not far from the melting point T_m. The material coming out of the extrusion machine in the shape of a tape is received by a turning roll with a flat perimeter rotating with a velocity u_1 and forwarded to a second similar roll but rotating with a velocity u_2. Both rolls are heated so as to be maintained at constant temperatures throughout the process. We have $u_1 < u_2$, so that between the first and the second roll deformation of the material still in the molten state takes place. The solidification proceeds gradually so that stretching accelerates the crystallization process in addition to providing orientation.

The specimens obtained by simple extrusion are in the form of films with a width of 14 mm and a thickness of 1.15 mm. The specimens obtained by Sodem are films with a width between 4.6 and 7.1 mm and a thickness between 0.28 and 0.42 mm; they are characterized by the draw ratio

$$\lambda = (\varepsilon + 1) \tag{1}$$

where the engineering strain $\varepsilon = (l - l_0)/l_0$, where l is the current length and l_0 the original length of the specimen.

A method similar to Sodem has already been applied to LDPE (low-density PE) blended with HDPE[26], but the paper in question does not describe the procedure used. Moreover, working with pure HDPE rather than with blends provides a better chance of understanding the connection between deformations obtained by Sodem and the resulting properties. This, in turn, should make possible later development of improved blends.

Mechanical testing procedures

Tests of three kinds were conducted: tension, stress relaxation and dynamic mechanical analysis (d.m.a., also known as d.m.t.a. (dynamic mechanical thermal analysis)). A Zwick-1444 universal machine equipped with a Brabender thermo-kryo chamber maintaining constant temperature within ±1 C was used for both tensile and stress relaxation experiments. Tensile testing was performed isothermally at temperatures ranging from 20°C to 120°C in 20°C intervals at the deformation rate of $20\,mm\,min^{-1}$, with a distance of 50 mm between the grips. The deformations were measured with an extensometer, with the electronic control system outside the chamber and thus unaffected by the probe temperature. The tensile modulus E was determined by the usual procedure from the slope of the initial part of the stress *versus* strain curve. Stress relaxation was determined in the range −50 to +120°C; in each case a constant tensile strain $\varepsilon = 0.025$ was imposed instantaneously and the experiment conducted for 10^3 s.

D.m.a. was performed using a Rheovibron DDV-III-EP viscoelastometer in the temperature range −150°C to +130°C. The frequencies $\omega = 3.5$, 11.0, 35.0 and 110 Hz were chosen. Five specimens were studied in each case in all three kinds of tests; the results reported below pertain to averages.

RESULTS AND DISCUSSION

Tensile results

The results of tensile testing at 20°C and at the strain rate $\dot{\varepsilon} = 0.004\,s^{-1}$ are summarized in *Table 1*. A word on pressure or stress units is appropriate at this point since so many are in use. The international system of units (SI) has established the joule, J, as the unit of energy. Unfortunately, the creators of SI defined a force unit called a newton, $N = J\,m^{-1}$, and also a unit of pressure called the pascal, $Pa = N\,m^{-2}$. Using N and Pa, one has to calculate back and forth into units containing J. Actually, the only convenient unit of pressure which minimizes recalculations is $J\,cm^{-3}$; it has been used, for instance, by Flory[27]. Fortunately, $1\,J\,cm^{-3} = 1\,MPa = 1\,MN\,m^{-2} = 10^7\,erg\,cm^{-3} = 10^7\,dyne\,cm^{-2} = 10\,bar = 9.86923\,atm = 145.04\,psi$. The results obtained at other temperatures will be discussed in conjunction with d.m.a. results below.

Some thermal (heat capacity C_p) and structural characteristics of the materials are included in the same table. The latter (degrees of orientation in crystalline and amorphous phases) have been obtained by wide-

Table 1 Results of tensile testing at 20°C and some other characteristics of the materials as a function of the draw ratio λ

	λ					
	1.0	5.5	7.5	9.1	10.9	12.2
Density, ρ (g cm^{-3})	0.9520	0.9575	0.9605	0.9615	0.9620	0.9620
Elastic modulus, E ($\times 10^{-3}$)(J cm^{-3})	1.07	3.60	4.60	5.70	6.20	7.10
Tensile strength, σ_m ($\times 10^{-3}$)(J cm^{-3})	–	0.20	0.25	0.30	0.32	0.37
Relative elongation at fracture (100%), ε_f	–	94	57	41	30	13
Degree of crystallinity (100%), d_{cr}	0.50	0.54	0.55	0.57	0.60	0.65
Degree of orientation in the crystalline phase, s_{cr}	–	0.95	0.95	0.95	0.96	0.96
Degree of orientation in the amorphous phase, s_{am}	–	0.91	0.92	0.91	0.91	0.92
Specific heat capacity, C_p (J g^{-1} K^{-1})	170	175	–	178	181	183

angle X-ray scattering (WAXS) using Ni-filtered Cu K_α radiation. We note the increase of the degree of crystallinity with the draw ratio, which was expected from earlier work. For instance, Choy and Leung[28] subjected HDPE to drawing up to $\lambda = 25$ and found a similar increase in crystallinity. Their study of thermal conductivity shows that, even at such high values of λ, crystalline bridges are separated by amorphous regions. The crystallinity increase caused by drawing would be less pronounced in PEs with lower densities and more branching.

Inspection of the table shows, first of all, that the elastic modulus E, the tensile strength σ_m, the degree of crystallinity d_{cr} and the specific heat capacity C_p all increase with increase in draw ratio λ. The density ρ first also increases with λ, but for $\lambda > 10$ reaches a plateau. By contrast – and as expected – the strain (relative elongation) at fracture ε_f decreases when λ increases. We conclude that the Sodem procedure accomplishes its basic objective of enhancing the mechanical properties. Over the λ range investigated the modulus of elasticity increases to some 660% of the value for the specimens which were not subjected to the Sodem procedure. The modulus values at the same draw ratios are comparable to those obtained by Mead *et al.*[14] for their HDPE extruded at 120°C and subjected to solid-state drawing (Figure 9 in ref. 14).

The Sodem molten state procedure has fairly evident advantageous traits from the point of view of its industrial implementation. If, for reasons related to a particular application, the strain at fracture is a concern, then a value of λ inside the λ range investigated by us can provide a compromise.

Time–temperature correspondence and the shift factor

As mentioned earlier, we apply the time–temperature correspondence principle to predict mechanical properties of viscoelastic materials at a given temperature over many decades of time from short-term experiments performed at several temperatures[15–18]. The temperature shift factor necessary for the prediction, $a_T = a_T(T)$, can be either measured or calculated, and there is a calculation procedure reported by Williams, Landel and Ferry (WLF) in 1955[29]. However, as discussed by Ferry himself[15], the equation is expected to work well at temperatures around $T_g + 50$ K, where T_g is the glass transition temperature, but not at or below T_g, nor at temperatures $T > T_g + 100$ K. Therefore, in general an equation usable in a wide temperature range would be desirable. There is an equation derived by one of us[19,20] relating a_T to the temperature T via the reduced volume $\tilde{v}$ (or free volume v^f), namely

$$\ln a_T = A + B/(\tilde{v} - 1) \tag{2}$$

where A and B are constants characteristic for a given viscoelastic material, and B comes from the Doolittle viscosity relation. A convenient choice, which possibly might be applicable to a number of polymers, is $B = 2.303$ (ref. 24). The reduced volume is defined as

$$\tilde{v} = v/v^* \tag{3}$$

The quantities featured in equation (3) can be defined at the molecular level (per chain segment) or, more conveniently for practical calculations, they can be specific quantities per gram of the material. v^* is the characteristic (also called incompressible or hard-core) volume, used extensively by Flory and collaborators in dealing with thermophysical properties; see for instance refs 30 or 31. We believe[19,20,24,25] that the concept of free volume v^f defined by

$$v^f = v - v^* \tag{4}$$

is equally useful for dealing with viscoelastic properties.

Equation (2) is fairly general; to use it, one needs to make a specific assumption concerning the dependence of the reduced volume $\tilde{v}$ (or of the free volume v^f) on the temperature T. One such choice, particularly simple but otherwise without foundation, leads to the WLF equation[20]. Calculations of the impact transition temperatures as a function of the stress concentration factors for LDPE have shown[20,32] that the WLF formula produces disastrous results at low temperatures. Virtually all other choices are better. Investigating a series of polyurethanes, we have obtained good results[24] with the Hartmann equation of state. That equation is known to be applicable to a large range of materials including polymer solids and liquids[21–23] and has the form

$$\tilde{P}\tilde{v}^5 = \tilde{T}^{3/2} - \ln \tilde{v} \tag{5}$$

Here

$$\tilde{P} = P/P^*; \qquad \tilde{T} = T/T^* \tag{6}$$

P denotes pressure; P^* and T^* are, like v^*, characteristic parameters for a given material, providing a generalized (reduced) form of the equation. T^* constitutes a measure of the strength of interactions in the material. High values

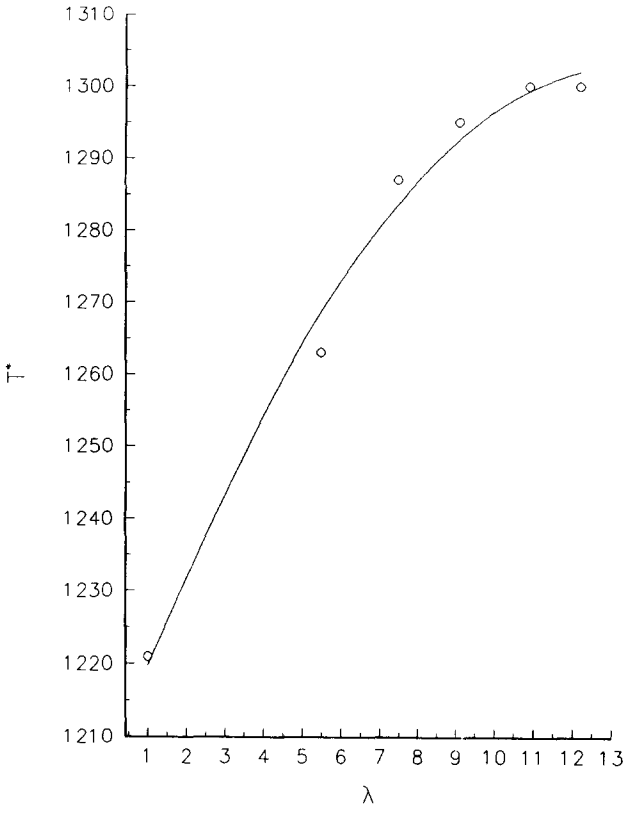

Figure 1 The characteristic temperature T^* as a function of the draw ratio λ. (○) Experimental points; the continuous line calculated from equation (8)

of T^* correspond to strong intermolecular or intersegmental interactions; for this reason T^* is quite important, for instance for properties of PLC-containing systems[33–37]. Since our experiments were conducted at atmospheric pressure, $P \approx 0.1\ \mathrm{J\,cm^{-3}}$, the term containing $\tilde{P}$ in equation (5) is negligible, and we have simply

$$\tilde{v} = \exp[\tilde{T}^{3/2}] \tag{7}$$

which can be substituted into equation (2).

To use equation (2) in conjunction with equation (7), we need to know the value of the characteristic temperature. For a material that did not undergo structure-changing deformations such as drawing, that is for a constant λ (including $\lambda = 1$), both v^* and T^* can be obtained from a set of experimental $v(T)$ data, or alternatively from a single value of v plus $\alpha(T)$ data, where the isobaric expansivity $\alpha = V^{-1}(\partial V/\partial T)_P$. Hartmann and Haque[22] have already analysed reliable experimental data for a number of polymers in the solid state and found $T^* = 1221$ K for HDPE, the value which we shall use for $\lambda = 1$ in computations reported below.

For $\lambda > 1$ we have developed the following approach. By definition, the hard-core volume v^* is a constant, corresponding to the situation when the entire free volume has been 'squeezed out'; see equation (4). However, since T^* represents the energetic situation in the system, interaction energies in general depend on the interparticle distance. Therefore, T^* necessarily changes with the extent of orientation in the material and the draw ratio λ. From equation (7), by using the experimental value of density for $\lambda = 1$ from *Table 1* and the value of T^* of Hartmann and Haque, we have obtained for our PE the value of $v^* = 0.9339$, which is within 2.5% of the value of $v^* = 0.9586$ for their PE. Then we have used our value of v^* and the remaining densities from *Table 1* to compute the characteristic temperature as a function of the draw ratio. The results are shown in *Figure 1*. The continuous line corresponds to the quadratic equation

$$T^* = f_0 + f_1\lambda + f_2\lambda^2 \tag{8}$$

with $f_0 = 1205.9$, $f_1 = 14.3$ and $f_2 = -0.53$. As expected, drawing increases first the degree of orientation – and therefore T^* – at a high rate; later on, when a considerable degree of orientation has already been acquired, the increase of T^* with λ becomes slower. Hartmann and Haque[22] also analysed data for linear PE, in which a high degree of orientation is expected. Indeed, in this case they have obtained $T^* = 1829$ K, in agreement with the trend shown in *Figure 1*.

Stress relaxation results

As indicated in Experimental, stress relaxation was determined under a constant tensile strain $\varepsilon = 0.025$ at a number of temperatures for specimens deformed to various extents by the Sodem procedure. For brevity we do not display individual experimental curves, but we show in *Figure 2* three master curves for different λ values ($10^3\ \mathrm{J\,cm^{-3}} = 1$ GPa).

In 1965 Kubát[38] had already demonstrated that the stress relaxation curves of vastly different materials have a common shape: an initial nearly horizontal part, a large central descending part, and then another part reaching a plateau corresponding to the internal stress σ_i. Our own curves also show the same shape. To explain it, Kubát and collaborators[39–44] developed a cooperative theory of stress relaxation. They assumed for simplicity a two-level system, with unrelaxed flow units in the upper level, so that there is a formal connection to the Bose–Einstein (B–E) distribution. The number n of unrelaxed units at any time t serves as the measure of stress σ, or more accurately of the difference $\sigma - \sigma_i$. The relaxation process consists of elementary events of varying multiplicity, so that clusters of different sizes are relaxing. The theory predicts a distribution of cluster sizes; B–E-type computer simulations render results close

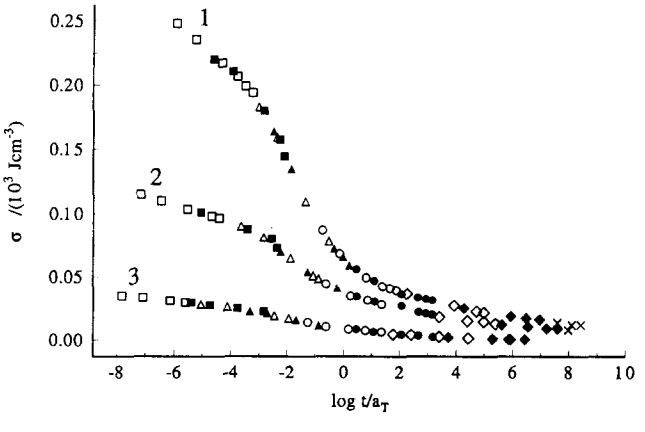

Figure 2 Master stress relaxation curves for HDPE at the reference temperature $T = 313.2$ K ($= 40$ C), constant tensile strain $\varepsilon = 0.025$ and at different values of the draw ratio: curve 1, $\lambda = 12.2$; curve 2, $\lambda = 5.5$; curve 3, material without predeformation ($\lambda = 1$). Experimental temperatures: □, −50 C; ■, −30 C; △, −10 C; ▲, 0 C; ○, 20 C; ●, 40 C; ◇, 60 C; ◆, 80 C; ×, 100 C

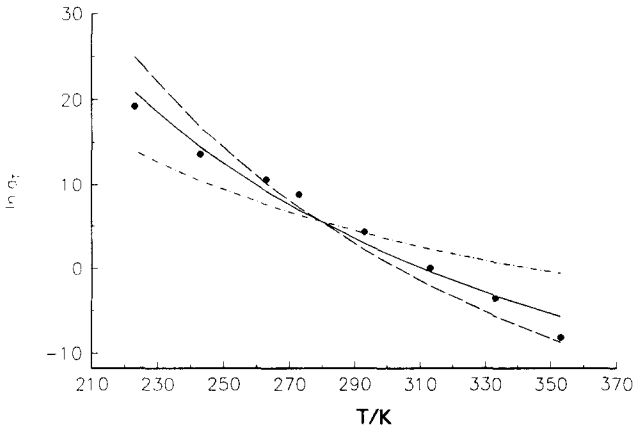

Figure 3 The temperature shift factor a_T as a function of temperature T obtained from stress relaxation experiments for HDPE with $\lambda = 1$. (●) Experimental values. The curves are calculated from equations (2), (7) and (8) as explained in the text

to, but not identical with, the theoretical distribution[45]. The numbers of smallest clusters found in simulations are somewhat higher than predicted by the original theory. Different simulations, namely using the method of molecular dynamics[46,47], conducted after the cooperative theory had been developed, confirm *a posteriori* its assumptions: the mechanism of stress relaxation consists of deformations taking place in the immediate vicinity of structural defects. These deformations are visible in simulations of metals as well as polymers; they correspond to cluster relaxations in the cooperative theory of Kubát and co-workers.

We see in *Figure 2* that the material with the highest degree of orientation ($\lambda = 12.2$) offers the highest resistance to the additional strain imposed in the stress relaxation experiment. The same material seems also to be the last to reach the plateau corresponding to the internal stress σ_i. It was reported above that the same material has the highest elastic modulus E and the highest tensile strength σ_m.

The previously undeformed material ($\lambda = 1$) shows the initial stress level σ_0 at very short times equal to approximately 12% of σ_0 for $\lambda = 12.2$. Moreover, in the present case σ_0 is not that far from the internal stress σ_i value. The material with the intermediate degree of orientation ($\lambda = 5.5$) shows, as expected, intermediate behaviour. For $\lambda = 1$, 5.5 and 12.2 we find, respectively, $(\sigma_0 - \sigma_i)/\sigma_0 = 0.74$, 0.76 and 0.84.

We also see in *Figure 2* that the time–temperature correspondence principle is well obeyed in the entire range of temperatures from -50 to $+100$°C and also in a wide range of deformation ratios $\lambda = 1$–12.2. To represent this behaviour, we have used equation (2) for the temperature shift factor a_T in conjunction with the Hartmann equation of state (equation (7)), equations (3) and (6) and the dependence of T^* on the draw ratio given by equation (8). First, we tried representing curves for each λ value independently using the method of least squares. In *Figure 3* we display the results for $\lambda = 1$. In one series of computations, A and B in equation (2) were both evaluated, with the result $A = -30.55$ and $B = 4.178$; see the continuous line in *Figure 3*. Then $B = 2.303$ was assumed, and only A evaluated (– · – ·), resulting in $A = -14.34$. Finally, $B = 2.303^2 = 5.304$ was assumed and A evaluated (– – –), giving $A = -40.28$. *Figure 3* shows that the experiments were less accurate at temperatures $T < 250$ K (a larger scatter of points), and probably above 330 K as well (*Figure 4* below shows evident errors for $T > 330$ K). Thus, taking the limited experimental accuracy into account, we find that satisfactory fit is obtained with both A and B evaluated. The predefined 'universal' values of $B = 2.303$ and $B = 2.303^2$ can serve only as zeroth-order approximations. These values were used before for a series of polyurethanes[24]. The results for $\lambda = 5.5$ and 12.2, not displayed here for brevity, lend themselves to analogous conclusions.

Equation (2) contains two terms on the right-hand side, and so far we have taken into account the effect of varying λ only in the second term. Therefore, the following approach was more interesting. Since we are dealing with the same material but oriented to a varying extent, we assumed that the A value is a function of the draw ratio λ. We further assumed that a universal value of B (not necessarily equal to 2.303 or 2.303^2 but independent of λ) may be used. Thus, we generalized equation (2) and for all stress relaxation curves of HDPE we represented the shift factor a_T as

$$\ln a_T = 1/(a + c\lambda) + B/(\tilde{v} - 1) \qquad (9)$$

Here the first parameter in the original shift factor equation is now $A = 1/(a + c\lambda)$; a and c are constants characteristic for a given material but independent of the degree of orientation and of temperature. Parameters a and c do not affect the shape of the $a_T(T)$ curve. The denominator of the first term in equation (9) represents a measure of the orientation. More specifically, a higher draw ratio results in a smaller number of chain conformations available to the material. With less conformations, the temperature effect on the number of conformations is smaller as well, which lowers the temperature shift factor. The temperature dependence of a_T is implicit in equation (9) but explicitly given by equation (7). The dependence of the second term in equation (9) on λ is also implicit, given by equation (8) in conjunction with the definitions in equations (3) and (6).

The results of computations using equation (9) in conjunction with equations (7), (8), (3) and (6) are shown

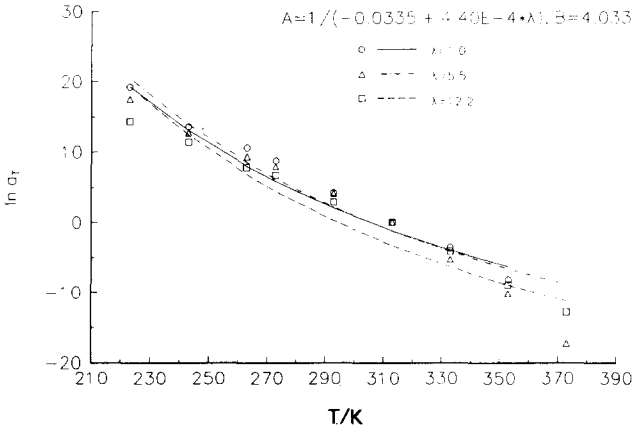

Figure 4 The temperature shift factor a_T as a function of temperature T obtained from stress relaxation experiments for HDPE with $\lambda = 1$ (○), $\lambda = 5.5$ (△) and $\lambda = 12.2$ (□). Curves calculated using equations (9), (7) and (8) as explained in the text

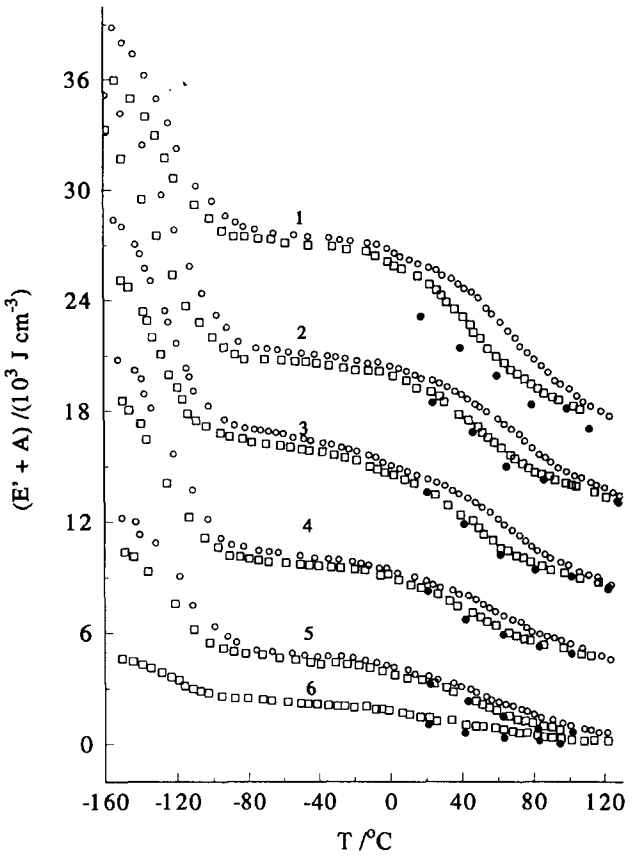

Figure 5 Dynamic modulus E' as a function of temperature T for the frequencies 3.5 Hz (□) and 110 Hz (○). Quasi-static elastic modulus E is also shown (●). Curve 1, $\lambda = 12.2$, the vertical shift $\Delta E' = 16.0 \times 10^3$ J cm^{-3}; curve 2, $\lambda = 10.9$, $\Delta E' = 12.0 \times 10^3$ J cm^{-3}; curve 3, $\lambda = 9.1$, $\Delta E' = 8.0 \times 10^3$ J cm^{-3}; curve 4, $\lambda = 7.5$, $\Delta E' = 4.0 \times 10^3$ J cm^{-3}; curve 5, $\lambda = 5.5$, $\Delta E' = 0$; curve 6, $\lambda = 1$, $\Delta E' = 0$. In the figure, $A = \Delta E'$

in *Figure 4*. The least-squares common value of $B = 4.033$ (approximately halfway between the two supposedly 'universal' values); $a = -0.0335$ and $c = 0.000440$. We observe that an increase of the draw ratio at a given temperature results in a decrease of a_T, in agreement with both the first term in equation (9) and with equation (8). A certain scatter of the experimental points at the extremes of the temperature range is clear; at high T values ($T \geqslant 330$ K) the shift factors for $\lambda = 5.5$ are lower than those for $\lambda = 12.2$, while throughout most of the range they are between the values for $\lambda = 1$ and $\lambda = 12.2$. Taking into account the experimental accuracy, we find that equation (9) in conjunction with equations (7) and (8) provides an entirely satisfactory fit of the temperature shift factor of HDPE as a function of both T and λ.

Dynamic mechanical results

D.m.a. experiments were performed as described above. The results were analysed in terms of one of the standard formulae (see for instance ref. 17)

$$\tan \delta(\omega) = E''(\omega)/E'(\omega) \qquad (10)$$

where δ is the angle by which strain lags the imposed stress, $\tan \delta$ is usually referred to as the loss tangent, E' is the storage modulus and E'' the loss modulus. While other parameters such as the dynamic complex modulus $E^*(i\omega) = E'(\omega) + iE''(\omega)$ are also widely used, we find working with E' and $\tan \delta$ convenient. In *Figure 5* we show E' values as a function of temperature T for two frequencies ω differing by two orders of magnitude, namely 3.5 Hz and 110 Hz, for several draw ratios λ. For comparison, we include in the same figure values of the elastic tensile modulus E. Because of overlaps, we have improved clarity by shifting vertically curves other than those for $\lambda = 5.5$ and $\lambda = 1$; the amounts of the shift $\Delta E = A$ are indicated in the legend.

We have already reported some of the quasi-static tensile testing results in *Table 1*. Parallel to the results displayed in that table for the elastic modulus E, the dynamic storage modulus E' increases with the draw ratio at all temperatures. At the temperature of 20°C we find that the storage modulus E' for $\lambda = 12.2$ at $\omega = 3.5$ Hz represents approximately 600% of the value for $\lambda = 1$ and at $\omega = 110$ Hz some 620% of the value for the undrawn material.

Possibly the most striking result found on *Figure 5* is the fact that E is so close to E', except (as expected) for the highest draw ratio $\lambda = 12.2$. We know, of course, that in principle E' represents the elastic (as contrasted with the viscous) constituent of the response of the viscoelastic material to dynamic loading. However, it is gratifying to see the agreement between two vastly different, but apparently both accurate, experimental procedures. At the same time, we recognize the limitations of the correspondence between E and E': at the highest draw ratio and at relatively low temperatures the values of E are *lower* than those of E'. These differences are even larger when the frequency ω of dynamic loading increases. The material subjected to periodic loading offers more resistance to deformation than in simple tension, and a frequency increase amplifies that resistance. In addition to the time–temperature correspondence principle invoked repeatedly in the present paper, *Figure 5* constitutes one more confirmation of the temperature–frequency correspondence, where high values of ω correspond to low values of T.

Consider now curves 3–6 for low draw ratios; the differences between E and E' here are largely negligible. Curves 1 and 2 show that more orientation enhances the difference between the quasi-static and dynamic responses. Moreover, we observe that the temperature increase has two effects. First, as expected, increased thermal energy in the material increases chain mobility and lowers the moduli. Second, the increase in mobility apparently destroys some of the orientation induced by drawing. This is reflected both in the modulus decrease and in the convergence of E and E' values visible at higher temperatures.

As discussed in some detail by Popli and co-workers[48], PEs undergo several solid-state relaxational transitions: γ between -150 and -120°C, β between -30°C and $+10$°C and α between $+30$ and $+120$°C. These authors explain the β transition in terms of relaxations of chain sequences located in the interfaces between the crystalline and amorphous regions. There are several ways to study the effects of solid-state relaxations on mechanical behaviour. For instance, there is a sophisticated procedure developed by Schlosser and his colleagues[49] which involves decomposition of relaxation effects into a number of overlapping functions corresponding to individual mechanisms. We have applied a simple and fairly obvious procedure of plotting a relative mechanical property as a function of temperature, that is, a quantity

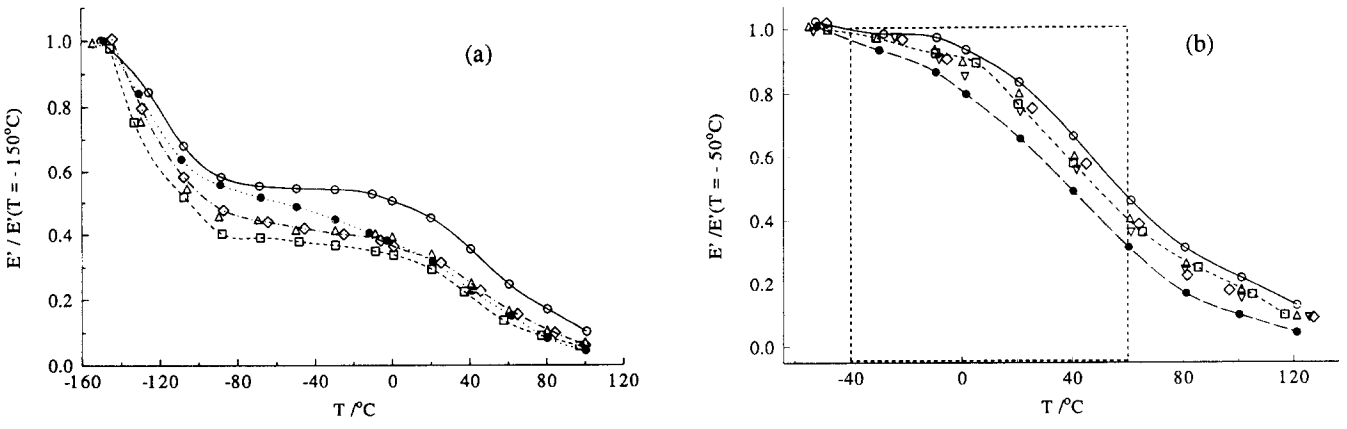

Figure 6 Relative storage modulus E'_{rel} defined by equation (11) at the frequency $\omega = 3.5$ Hz for two different reference temperatures: (a) $T_0 = -150$ C; (b) $T_0 = -50$ C. Symbols correspond to different draw ratios: $\lambda = 1$ (●), 5.5 (□), 7.5 (◇), 9.1 (▽), 10.9 (△) and 12.2 (○). The enclosed region in (b) corresponds to the usual service temperatures from −40 C to +60 C

normalized with respect to the same property at a reference temperature T_0. We have done this with the storage modulus

$$E'_{rel}(T) = E'(T)/E'(T_0) \qquad (11)$$

for two reference temperatures, namely $T_0 = -150$°C and −50°C. The results for the frequency $\omega = 3.5$ Hz are shown in *Figure 6a* and *b*, respectively.

The curves in *Figure 6a* for $T_0 = -150$°C can be analysed by starting with that for $\lambda = 1$. We see that an increase of the draw ratio to 5.5 lowers the relative storage modulus. Then E'_{rel} begins to increase, with the results for $7.5 \leqslant \lambda \leqslant 10.9$ forming a virtually single curve. For the highest value $\lambda = 12.2$ a distinct further increase in E'_{rel} is observed.

By contrast, the curves in *Figure 6b* for $T_0 = -50$°C show that E'_{rel} is a function of the draw ratio. Returning now to $T_0 = -150$°C, we note that it is below all three solid-state relaxational transitions, γ, β and α. Apparently the effects of drawing are then different than at a higher temperature such as −50°C.

So far we have dealt with the elastic behaviour in dynamic loading; we now turn to viscous behaviour. Tan δ is more often used than the loss modulus E''. We shall also follow the customary route, but the fact that tan δ as defined by equation (10) is a ratio of two moduli has to be kept in mind at all times. To evaluate the effects of the Sodem procedure, we consider first results for unstretched materials ($\lambda = 1$) at 12 different temperatures. The tan δ values as a function of the logarithmic reciprocal frequency $\log \omega^{-1}$ are shown in *Figure 7*.

The results in *Figure 7* are such as would be expected for the simple unstretched extrudate. First, the increase in temperature should increase the loss modulus E'' and consequently increase tan δ, as indeed is observed. Second, we already invoked above the fact that high values of ω correspond to low values of T, and *Figure 7* constitutes one more manifestation of this fact: a decrease in ω, that is an increase in ω^{-1}, corresponds to an increase in T, and tan δ increases from left to right. The curves at low temperatures are concave, but at high temperatures, approaching the α transition of PE, they become convex.

In *Figure 5* we have seen an example of the temperature–frequency correspondence, but we dealt with two frequencies only. Now we have used results

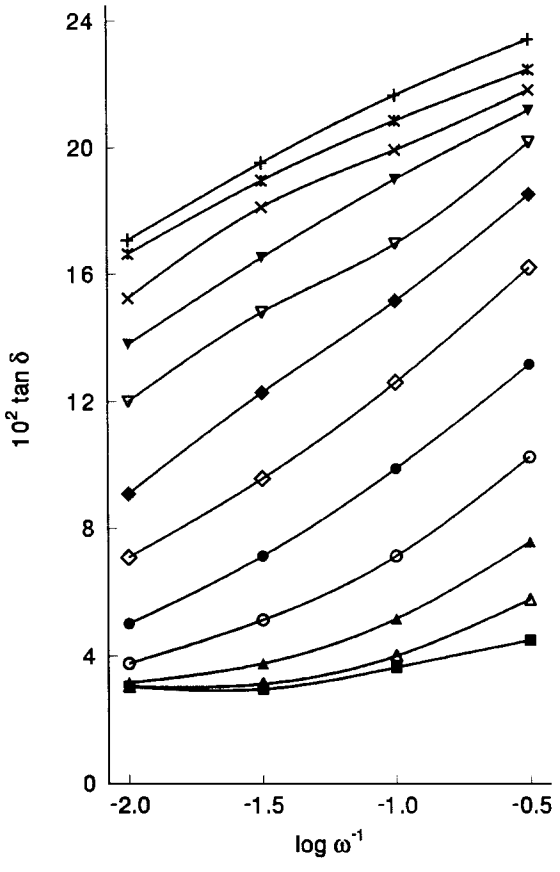

Figure 7 Tan δ as a function of logarithmic reciprocal frequency $\log \omega^{-1}$ for $\lambda = 1$ at several temperatures: 0 C (□); 10 C (■); 20 C (△); 30 C (▲); 40 C (○); 50 C (●); 60 C (◇); 70 C (◆); 80 C (▽); 90 C (▼); 100 C (×); 110 C (*); 120 C (+)

displayed in *Figure 7* for 12 temperatures, each over some decades of frequency. We have performed superpositions for the reference temperature $T_0 = 40$°C and thus created the tan δ *versus* log a_T/ω master curve shown in *Figure 8*.

Figure 8 shows that the temperature–frequency correspondence principle is also obeyed. We have analysed the experimental a_T (T) values obtained via the superposition procedure. We stressed above the fact that tan δ is a ratio of two moduli, therefore a_T (T) values obtained in creating *Figure 8* do not have to be equal to those obtained from stress relaxation experiments and reported

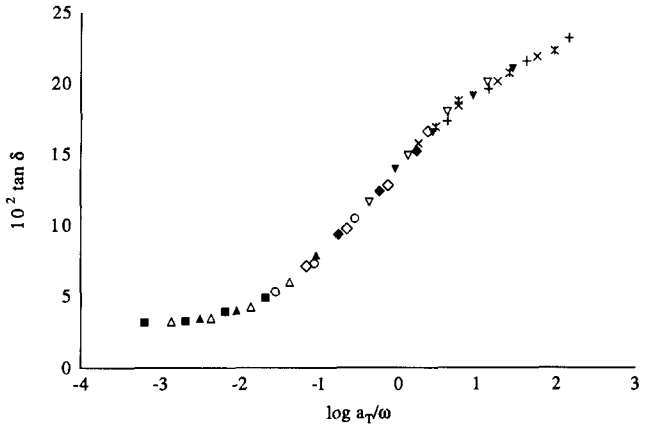

Figure 8 The master curve of tan δ *versus* $\log a_T/\omega$ for 40°C based on results shown in *Figure 7*. Symbols representing temperatures are the same as in *Figure 7*

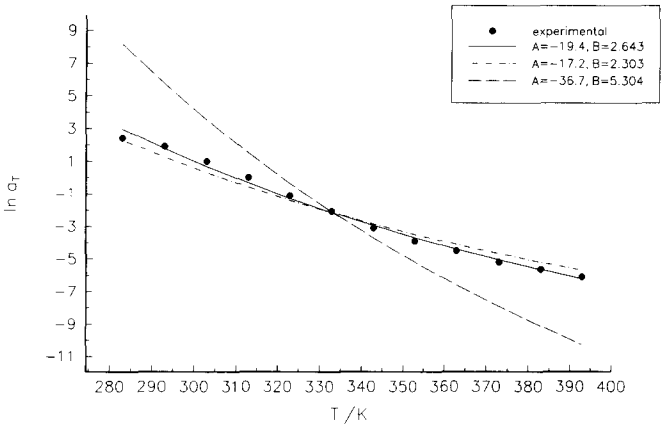

Figure 9 The temperature shift factor a_T as a function of temperature T obtained from d.m.a. tan δ results for HDPE with $\lambda = 1$. (●) Experimental values. The curves are calculated from equations (2), (7) and (8) as explained in the text

above as indeed turns out to be the case. PE is a semicrystalline polymer. In the third edition of his authoritative book, van Krevelen[50] notes that such polymers do not obey the WLF equation below their melting points. He discusses the application to semicrystalline polymers of an Arrhenius-type formula

$$U^{act} = R \ln a_T / (T^{-1} - T_0^{-1}) \qquad (12)$$

in which U^{act} is the so-called activation energy, which is supposed to be independent of the temperature. However, our calculations show that U^{act} varies in the temperature range we have investigated from 65 to 80 kJ mol^{-1}. Thus, while U^{act} is a convenient concept for the consideration of temperature effects on chain conformations and mobility, its physical significance can hardly be taken literally. The increase of U^{act} along with the temperature increase is probably related to structural changes which occur when approaching the α transition, in the interfacial regions in particular.

Given the unsatisfactory results of using equation (12), we have applied again equation (2) in conjunction with equations (7) and (8). The results are shown in *Figure 9*. The continuous line corresponds to evaluation of both A and B by the method of least squares (the values of these parameters are listed in the insert). Assumption of $B = 2.303$ resulted in the – · – · curve, while assumption of $B = 2.303^2$ resulted in the broken line. While the first choice is even better, it is clear that in this case taking $B = 2.303$ gives satisfactory results. In contrast, assuming $B = 2.303^2$ leads to unacceptable results.

Since one of the themes of this paper is the evaluation of the Sodem procedure, we have also performed analogous experiments and calculations for specimens with the highest value of the draw ratio. *Figure 10* is an analogue of *Figure 7*, but now for $\lambda = 12.2$. We see that a high level of orientation has complicated a simple picture which was visible in *Figure 7*. At lower temperatures we observe, as before, that a decrease in frequency ω results in an increase of the viscous response, reflected in the rise of tan δ. At 70°C we observe a maximum. At temperatures higher than 70°C we see that decreasing the frequency results in a decrease of tan δ. The last observation has to be related to the fact that lower frequencies allow the chains more time for conformational rearrangements, at higher temperatures in particular, a phenomenon somewhat akin to annealing. The changes that occur will eliminate some 'artificial' conformations created by the *force brute* during drawing. Apparently, the resulting configurations create a more regular alignment than before, more effective orientation, and a decrease in tan δ. We recall results from a statistical-mechanical analysis of PLCs[36]: oriented (in that case liquid-crystalline) sequences impart their orientation to flexible sequences 'trapped' between them.

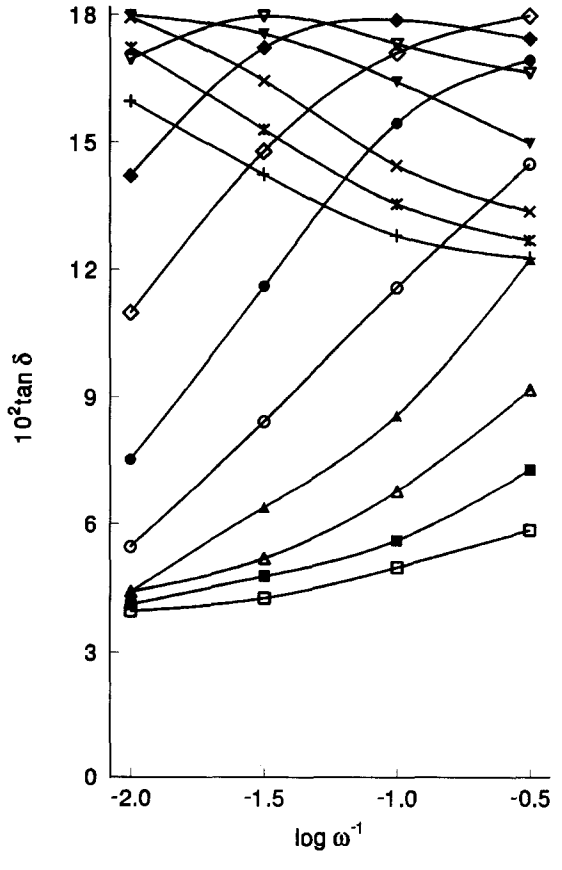

Figure 10 Tan δ as a function of logarithmic reciprocal frequency $\log \omega^{-1}$ for $\lambda = 12.2$ at several temperatures. Symbols representing the temperatures are the same as in *Figure 7*

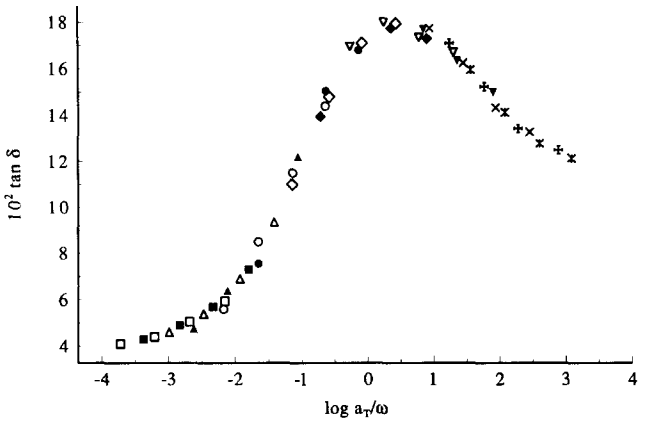

Figure 11 The master curve of $\tan\delta$ *versus* $\log a_T/\omega$ for 40°C based on results shown in *Figure 10*. Symbols representing the temperatures are the same as in *Figure 7*

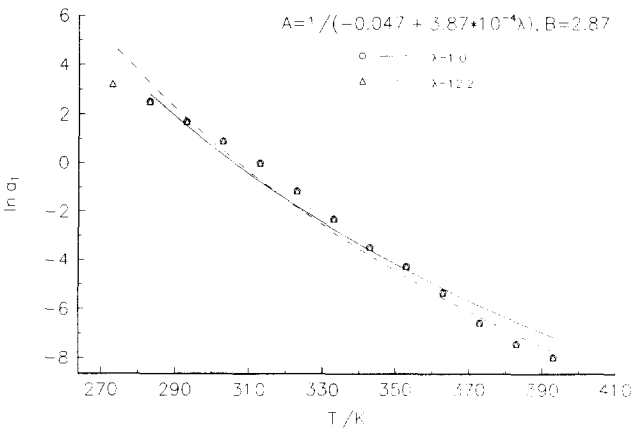

Figure 12 The temperature shift factor a_T as a function of temperature T obtained from d.m.t.a. $\tan\delta$ results. Experimental values: (○) $\lambda = 1$, (△) $\lambda = 12.2$. The curves are calculated from equations (9), (7) and (8) as explained in the text

Again, we have performed calculations of the activation energy U^{act}. For $\lambda = 12.2$ the variations of that energy in our temperature range are even greater, leading to almost doubling, namely from 60 to 106 kJ mol^{-1}. The achievement of mobility, as represented by $\tan\delta$, encounters a larger barrier in oriented specimens. Not only approaching the α transition but additionally the conformational rearrangements we have just discussed clearly invalidate the assumption of constant activation energy U^{act} in equation (12).

Similarly to previously, we have created the $\tan\delta$ *versus* $\log a_T/\omega$ master curve for $T_0 = 40$°C and $\lambda = 12.2$ shown in *Figure 11*, an analogue of *Figure 8*. The temperature–frequency correspondence is applicable at this high draw ratio as well. As expected from *Figure 10*, the curve has a maximum.

Comparisons of the pairs of figures under consideration (*Figures 7* and *8* respectively with *Figures 10* and *11*) can be performed also in a different way, relatively simple and at the same time complementary to the discussion above. Apparently, the α transition temperature has shifted to a lower value as a consequence of drawing. Thus, while for $\lambda = 1$ that transition was barely reached from one side (*Figure 8*), for $\lambda = 12.2$ it appears in the middle of *Figure 11*. Hartmann and co-workers, working with quantities such as shear modulus and frequency[51], established the existence of a relationship between the height and width of a relaxation. We are working with $\tan\delta$ as a function of $\log a_T/\omega$; comparison of *Figures 8* and *11* shows that drawing has resulted in narrowing the peak and at the same time in moving it to lower $\log a_T/\omega$ values.

We have applied equation (2) in conjunction with equations (7) and (8) to the shift factor a_T (T) values for $\lambda = 12.2$ obtained creating *Figure 11*. We do not display the results for brevity, but they are similar to those for $\lambda = 1$ in *Figure 9*. Now also, assuming independent A and B values gives good results, taking $B = 2.303$ still gives satisfactory results, while $B = 2.303^2$ gives clearly unacceptable results. Thus, in default of other information, the 'universal' value of $B = 2.303$ can be used.

Finally, given good results obtained for the shift factors from stress relaxation, we have again used equation (9) together with equations (7) and (8). The resulting parameters are $a = -0.0471$, $c = 0.000387$ and $B = 2.866$. Calculated and experimental values are shown in *Figure 12*. Clearly the generalized shift factor equation which takes into account the draw ratio in both terms is applicable to $\tan\delta$ *versus* $\log\omega^{-1}$ curves as well.

CONCLUDING REMARKS

We have found that the Sodem procedure leads to significant (over 600%) improvement of mechanical properties of HDPE. Sodem is relatively simple and easy to implement, and thus advantageous in comparison to other procedures with similar objectives.

Equation (2) for the temperature shift factor a_T[19,20] in conjunction with the Hartmann equation of state, equation (7), and with equation (8), produces a satisfactory representation of the $a_T(T)$ dependence. Even the assumption of the 'universal' value of the Doolittle constant, namely $B = 2.303$, gives results which can be used as the zeroth-order approximation. The characteristic temperature T^* available from experiments, or for instance from ref. 22, is also needed. For an unstretched material a single value of the shift factor a_T then makes possible via equations (2) and (7) predictions of the a_T (T) dependence, and of all quantities that can be derived therefrom. This is in contrast not only to the WLF equation, which is known to be inapplicable in the solid phase, but also to the Arrhenius-type equation (12) for which U^{act} changes considerably with temperature, and nearly doubles for stretched HDPE.

The present generalization of equation (2), namely equation (9) in conjunction with the Hartmann equation (7) and with equation (8), takes into account in two ways the extent of orientation as represented by the draw ratio λ. The first term in equation (9) deals with the fact that a drawn sample has less chain conformations available and therefore the shift factors are smaller in comparison to those for undeformed specimens. As discussed above, the second term deals with changes in intersegmental interactions caused by drawing. Equation (9) has the advantages of equation (2) but affords enhanced capabilities of extension over several decades of results of mechanical tests, including prediction of long-term behaviour from short-term tests.

ACKNOWLEDGEMENTS

Financial support for this work was provided by the Ford Motor Co., Detroit, via Industry–University Cooperative Research Center on Nanostructural Materials (IUCRC-NM) and by the Perkin–Elmer Corp. in the form of an equipment grant. Discussions with Professor Henryk Galina at UNT, Dr Bruce Hartmann of the Naval Surface Warfare Center, Silver Spring, MD, Professor Josef Kubát of the Chalmers University of Technology, Gothenburg, and with Dr Kevin P. Menard of Perkin–Elmer Corp, Stafford, TX, are appreciated. Professor C. L. Choy of the Chinese University of Hong Kong has provided us with his useful publications. Detailed constructive comments of two referees are also appreciated.

REFERENCES

1 Brostow, W. and Müller, W. F. *Polymer* 1986, **27**, 76
2 Brostow, W., Fleissner, M. and Müller, W. F. *Polymer* 1991, **32**, 419
3 Lustiger, A. in 'Failure of Plastics' (eds. W. Brostow and R. D. Corneliussen), Hanser, Munich, 1986, Ch. 16
4 Mathur, S. C. and Mattice, W. L. *Macromolecules* 1988, **21**, 1354
5 Runt, J. and Jacq, M. *J. Mater. Sci.* 1989, **24**, 1421
6 Lustiger, A. and Ishikawa, N. *J. Polym. Sci. Phys.* 1991, **29**, 1047
7 Hosoda, S. and Uemura, A. *Polym. J.* 1992, **24**, 939
8 Brostow, W., Hess, M. and López, B. L. *Macromolecules* 1994, **27**, 2262
9 Terselius, B., Gedde, U. W. and Jansson, J.-F. in 'Failure of Plastics' (eds. W. Brostow and R. D. Corneliussen), Hanser, Munich, 1986, Ch. 14
10 Coates, P. D. and Ward, I. M. *J. Polym. Sci. Phys.* 1978, **16**, 2031
11 Coates, P. D. and Ward, I. M. *Polymer* 1979, **20**, 1553
12 Kaito, A., Nakayama, M. and Kanetsuna, H. *J. Appl. Polym. Sci.* 1985, **30**, 4591
13 Gann, L. A., Marikhin, V. A., Myasnikova. L. P., Budtov, V. P. and Myasnikov, G. D. *Vysokomol. Soed. A* 1988, **30**, 573
14 Mead, W. T., Desper, C. R. and Porter, R. S. *J. Polym. Sci. Phys.* 1979, **17**, 859
15 Ferry, J. D. 'Viscoelastic Properties of Polymers', 3rd edn, Wiley, New York, 1980
16 Aklonis, J. J. and MacKnight, W. J. 'Introduction to Polymer Viscoelasticity', 2nd edn, Wiley, New York, 1983
17 Kenner, V. H. in 'Failure of Plastics' (Eds. W. Brostow and R. D. Corneliussen), Hanser, Munich, 1986, Ch. 2
18 Goldman, A. Ya. 'Prediction of the Deformation Properties of Polymeric and Composite Materials', American Chemical Society, Washington, DC, 1994
19 Brostow, W. *Mater. Chem. Phys.* 1985, **13**, 47
20 Brostow, W. in 'Failure of Plastics' (Eds W. Brostow and R. D. Corneliussen), Hanser, Munich, 1986, Ch. 10
21 Hartmann, B. *Proc. Can. High Polym. Forum* 1983, **22**, 20
22 Hartmann, B. and Haque, M. A. *J. Appl. Phys.* 1985, **58**, 2831
23 Hartmann, B. and Haque, M. A. *J. Appl. Polym. Sci.* 1985, **30**, 1553
24 Brostow, W., Duffy, J. V., Lee, G. F. and Madejczyk, K. *Macromolecules* 1991, **24**, 479
25 Brostow, W. *Makromol. Chem. Symp.* 1991, **41**, 119
26 Artemev, V. A., Goldman, A. Ya, Myasnikov, G. D. and Sulzhenko, L. L. *Vysokomol. Soed. A* 1985, **27**, 1047
27 Flory, P. J. *Faraday Soc. Disc.* 1970, **49**, 7
28 Choy, C. L. and Leung, W. P. *J. Polym. Sci. Phys.* 1983, **21**, 1243
29 Williams, M. L., Landel, R. F. and Ferry, J. D. *J. Am. Chem. Soc.* 1955, **77**, 3701
30 Flory, P. J. *Discuss. Faraday Soc.* 1970, **49**, 7
31 Flory, P. J. and Höcker, H. *Trans. Faraday Soc.* 1971, **67**, 2258
32 Brostow, W. and Macip, M. A. *Macromolecules* 1989, **22**, 2761
33 Flory, P. J. and Abe, A. *Macromolecules* 1978, **11**, 1119
34 Abe, A. and Flory, P. J. *Macromolecules* 1978, **11**, 1122
35 Jonah, D. A., Brostow, W. and Hess, M. *Macromolecules* 1993, **26**, 76
36 Blonski, S., Brostow, W., Jonah, D. A. and Hess, M. *Macromolecules* 1993, **26**, 84
37 Brostow, W. and Walasek, J. *Macromolecules* 1994, **27**, 2923
38 Kubát, J. *Nature* 1965, **204**, 378
39 Kubát, J. and Rigdahl, M. *Mater. Sci. Eng.* 1976, **24**, 223
40 Bohlin, L. and Kubát, J. *Solid State Commun.* 1976, **20**, 211
41 Högfors, Ch., Kubát, J. and Rigdahl, M. *Phys. Status Solidi B* 1981, **107**, 147
42 Kubát, J., Nilsson, L.-Å. and Rychwalski, W. *Res Mechanica* 1982, **5**, 309
43 Kubát, J. *Phys. Status Solidi B* 1982, **111**, 599
44 Kubát, J. and Rigdahl, M. in 'Failure of Plastics' (Eds W. Brostow and R. D. Corneliussen), Hanser, Munich, 1986, Ch. 4
45 Brostow, W., Kubát, J. and Kubát, M. J. *Mater. Res. Soc. Symp.* 1994, **321**, 99
46 Brostow, W. and Kubát, J. *Phys. Rev. B* 1993, **47**, 7659
47 Blonski, S., Brostow, W. and Kubát, J. *Phys. Rev. B* 1994, **49**, 6494
48 Popli, R., Glotin, M., Mandelkern, L. and Benson, R. S. *J. Polym. Sci. Phys.* 1984, **22**, 407
49 Schlosser, E., Schönhals, A., Carius, H.-E. and Goering, H. *Macromolecules* 1993, **26**, 6027
50 van Krevelen, D. W. 'Properties of Polymers', 3rd edn, Elsevier, Amsterdam, 1990, Ch. 13
51 Hartmann, B., Lee, G. F. and Lee, J. D. *J. Acoust. Soc. Am.* 1994, **95**, 226